Measuring the flow intrusion towards building areas during urban floods: Impact of the obstacles located in the streets and on the facade

Emmanuel Mignot, Loick Camusson, Nicolas Riviere

Measuring the flow intrusion towards building areas during urban floods: impact of the obstacles located in the streets and on the facade

Emmanuel Mignot[1], Loick Camusson[1], and Nicolas Riviere[1]

[1]Univ. Lyon, INSA Lyon, Ecole Centrale de Lyon, Université Claude Bernard Lyon I, CNRS, LMFA, UMR 5509, 20 avenue Albert Einstein, F-69621, VILLEURBANNE, France

January 22, 2020

1 Abstract

This paper provides, through laboratory experiments, the flow discharge passing from a flooded street to a building area through different types of damaged openings (a door, a window and a gate) along with a sensitivity analysis of this discharge to the presence of obstacles or facade details. Four flow regimes in the street are tested, representing a high or low street slope with a high and low water depth. These flows resemble that over rectangular side weirs, with the major difference that obstacles are usually located near the opening

Notations

b	Channel width (m)
C_d	Side weir discharge coefficient (-)
Fr_1	Froude number at channel centerline facing the upstream end of the opening (-)
h_1	Flow depth at channel centerline facing the upstream end of the opening (m)
h_3	Flow depth at channel centerline facing the downstream end of side weir (m)
h_d	Flow depth at channel centerline, 1m downstream from the center of the opening (m)
h_u	Flow depth at channel centerline 1m upstream from the center of the opening (m)
L	Length of side weir (m)
p	Crest height of side weir (m)
Q_d	Outlet discharge in the main channel (m^3s^{-1})
Q_u	Prescribed upstream discharge in the main channel (m^3s^{-1})
Q_w	Intrusion discharge (m^3s^{-1})
ΔQ_w	Intrusion discharge difference with an obstacle configuration vs without obstacle

in the street or on the facade. 26 configurations of obstacles are then included, one after the other, and their impact on the flow intrusion is measured. For the flow cases without obstacle, the agreement of the semi-analytical equations available in the literature strongly varies from one equation to another. On the other hand, the 220 tested flow cases reveal that the location of the obstacle with regards to the opening strongly modifies the impact of the obstacles, that increasing the Froude number tends to increase the impact of the obstacles and that obstacles have a higher impact on the intrusion discharge through a window than to a door or a gate. Finally we conclude that the largest obstacles (typically parked cars) located in the vicinity of openings should be somehow included in operational numerical models that calculate urban floods for a fair prediction of the intrusion discharge.

2 Keywords

Urban flood; flow intrusion; side weirs; obstacles

3 Introduction

Between 1995 and 2015, floods accounted for 43 % of all weather related disaster events, affecting 2.3 billion and killing 157,000 people (UNISDR and CRED, 2015). Besides, in 2018 four flood events were among the top ten deadliest disaster events (Guha-Sapir, D., 2018). Being prepared and managing flooding events is then of high priority for authorities (Fang, 2016). Besides, the number of inhabitants living within urban areas keeps increasing : from 33.35 % of the world population in 1980 to 55.27 % in 2018 (United Nations Population Division, 2018) and up to a prevision of 70% in 2050 (Gross, 2016). This growing urbanization results in an increase of flooding risk within urbanized areas (Chen et al., 2015). Among the tasks aiming at dealing with such risk events, the zonation of flood risk level throughout the city (Wu et al., 2015) and the planning of citizen evacuation (Baba et al., 2017) are getting more and more attention. These tools are generated by post-processing the urban flood simulation scenarios computed using operational 2D shallow water equation models (Mignot et al., 2006).

The complexity and efficiency of these operational numerical tools has been strongly increasing for the last 15 years, reproducing more and more flow processes, such as (i) the flow exchanges between the flooded streets and the underground sewer network (Chang et al., 2018) or large areas such as malls or metro (Takayama et al., 2007); (ii) the flow interactions with urban furniture (Bazin et al., 2017) or (iii) planing the evacuation of inhabitants (Ishigaki, 2008). However, Mignot et al. (2019) recently listed the remaining flow processes taking place during urban flood events, not reproduced by operational 2D numerical model. For instance, Mignot et al. (2019) state that no pollution dispersion model was developed and tested to reproduce urban flood pollution releases. Similarly, these authors state that the operational numerical models reproduc-

ing urban floods do not simulate the flow entering the building areas (individual houses or building blocks), but rather consider the facades along the streets as impervious. This is odd, given the level of damage and risk of the flow invading the building areas (industrial, commercial and living spaces) where material can be strongly damaged (such as all electronic tools), walls and furniture can rapidly rot and strong risk of drowning exist for inhabitant occupying the buildings.

We believe (1) that operational numerical models that simulate urban floods to assess the spatial distribution of level of risk should reproduce the flow invading building areas and (2) that the validation of these models (analytical or empirical) requires experimental data. Present work then aims at modeling experimentally flow intrusions from a flooded street towards a building for future calibration/validation of models to be developped. A few authors dedicated their research to the flow intrusion within a single building with openings, either experimentally (Liu et al., 2018), or numerically (Gems et al., 2016); or within a group of buildings facing the incoming flow in a highly simplified configuration within a straight channel (Zhou et al., 2016). To the best of our knowledge, the only work dedicated to realistic flow intrusions, in partially urbanized area, was performed by Sturm et al. (2018), with large separated buildings with open doors and windows in a village adjacent to an overtopping torrent. However, the process of flow within a highly urbanized area, where the water flows in a street network and passes from the streets to the building areas, was not studied, neither experimentally or numerically.

During an urban flood, part of the water flowing in the streets enters the buildings through, what we will call here "openings". The most-common ones are doors, windows and gates. Openings are usually initially closed. During frequent floods, flow intrusion thus takes place through leakage on the sides

of openings, or through overflows from sewer surcharges, for example through plumbing and sanitary elements. During extreme flood events, the submerged openings can open by themselves, get damaged, or be entirely removed. In these last cases, the flow through the openings is expected to behave similarly as that over side weirs (as long as the level of water does not reach the top of the opening) of quite large thickness, typically that of the wall. One first objective of the present work is then to evaluate if the flow discharge through openings within urban facades can be predicted by available side weir formulas from the literature.

One concern, nevertheless is that the flow through openings is expected to be affected by the obstacles located in the street and on the facade, such as trees, mailboxes, parked cars, bus shelters, traffic lights... depending on their sizes and locations with regards to the facade and to the opening. How the obstacles alter the flow discharge passing from the streets to the buildings is of major importance. Indeed, if their impact on the intrusion discharge is high, these obstacles must be included in the topography of the 2D flood simulations or in the semi-analytic weir formulas coupled to the 2D models; oppositely, if their impact is negligible, they can be discarded. Consequently, it is highly important to identify, for each type of opening and flood regime, the magnitude of impact of all obstacles on the intrusion discharges.

The present work finally aims at:

- investigating the processes governing the flow intrusion from a flooded street towards a building area,
- evaluating the capacities of existing analytical formulas to predict the intrusion discharge through facade openings, for configurations without obstacles
- quantifying the impact of obstacles typically encountered in a street or on

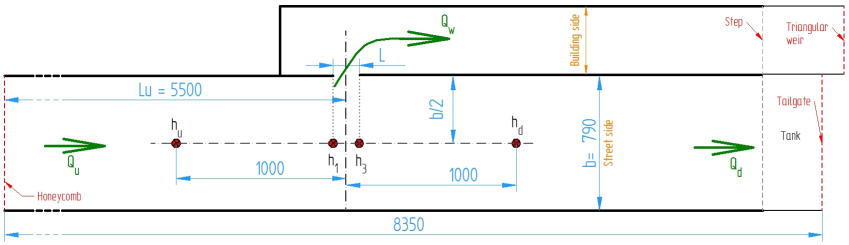

Figure 1: Experimental set-up with all dimensions in mm.

a facade on the flow intrusion discharge

- generating a database of flow intrusion towards building areas during urban floods.

This work will then provide for numerical models both a database and a sensitivity analysis dedicated to the intrusion towards buildings during urban floods.

The paper is organized as follows. The first section introduces the experimental set-up and measurement devices used in the present research, along with the research methodology, including a list of tested (i) openings, (ii) flow configurations and (iii) obstacles. The second section presents the flow patterns of flow intrusion without any obstacle and evaluates the capacities of existing analytical formulas to predict the intrusion flow discharge for all tested openings and flood regimes. The following section then evaluates the impact of different obstacles on this intrusion discharge. The paper ends up with a discussion regarding the necessity to include obstacles in operational models of flood simulation.

4 Experimental setup and methodology

4.1 Experimental set-up

The experiments are performed at the Laboratory of Fluid Mechanics and Acoustics (LMFA) at the University of Lyon (Insa-Lyon, France). The facility reproduces a highly simplified 1:12 scale model of a street and an adjacent facade within which various openings can be included to reproduce the intrusion flow from the flooded street towards a building area. Neither the layout within the building area nor the possible backward flow from the building area to the street are reproduced here for sake of simplicity.

A sketch of the experimental setup is shown in Fig. 1. It consists of a 8.35 m long and 0.79 m wide straight and smooth open-channel of rectangular cross-section and constant slope 1.8/1000, referred to as *street side* on the figure. The topography of the street profile is kept horizontal, the elevation of the sidewalk being neglected. The discharge Q_u entering the channel upstream is measured in the pumping loop using one of the two available electromagnetic flowmeters (Endress-Hauser): the first one is in the range $Q = 5 - 40$ L/s with an uncertainty of 0.2 L/s, while the other is $Q = 0 - 5$ L/s with an uncertainty of 0.05 L/s.

The upstream boundary condition consists of a grid buffer and a honeycomb with small mesh (0.5 cm alveolus) in order to stabilize the inflow. Furthermore, a sharp crested tailgate at the outlet of the channel is used to adjust the water depth to the desired value in front of the opening. Water depths along the center of the channel (h_u, h_1, h_3, h_d from up- to downstream on Fig. 1) are measured using a digital point gauge. The left wall of the channel (along $y = 0$ axis) is made of a 1 cm thick PVC plate within which openings can be machined at a distance $L_u = 5.5$ m downstream from the channel entrance. The center of the axis system (x, y, z) is located at the bottom of the center of the opening along

the street side of the PVC plate, with x the streamwise axis, y the transverse axis towards the street side and z the direction perpendicular to the bed.

As the intrusion discharge Q_w passing through the opening flows towards the outlet of the *building side*, it is measured using a previously calibrated triangular weir. The corresponding upstream flow elevation is measured using an ultrasonic sensor. Note that a step upstream from the triangular weir along with the 1.8/1000 slope of the *building side* prevent from any backward effect of the weir affecting the intrusion discharge. Finally, the outlet discharge downstream from the street is obtained by resting the two measured discharges: $Q_d = Q_u - Q_w$

For a few configurations, the surface velocity field in street side near the opening is measured by LSPIV (Large-scale particle image velocimetry) with a camera located 1.5 m above the flume, recording images of the free-surface seeded with dry sawdust at a frequency equal to 50 frames per second. Also, 2D fields of the water level are measured in the same area using an ultrasonic sensor fixed on an automated mobile car moving along both x and y directions.

4.2 List of openings (Op)

By looking at photos of highly urbanized areas, it appears that most openings connecting streets to building areas are windows, doors and gates. As these openings are damaged/removed, they leave a large open space available for flow intrusion. To model these configurations, 4 types of openings are considered and sketched in Fig. 2: Op 1 an open window, Op 2 is an open/damaged door, Op 3 a wider window and Op 4 represents a simplified closed gate with a grid on top. These openings are created in the model by simply drilling the vertical PVC plate at the interface between the street and the building, so that the intrusion water can freely flow through the white areas of each opening in Fig. 2

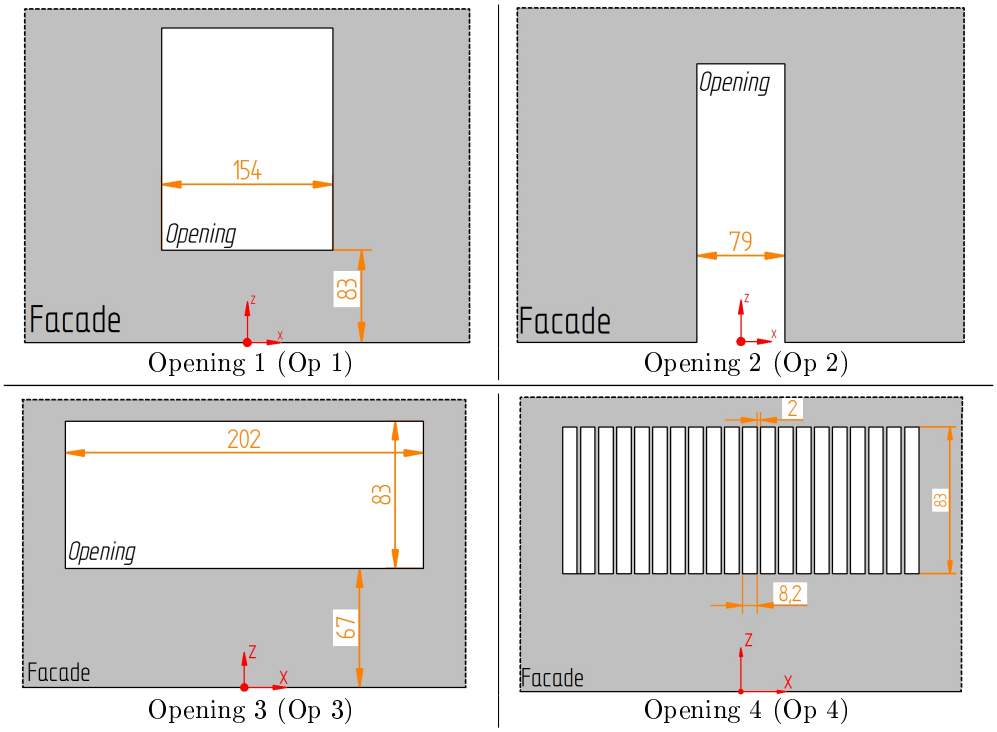

Figure 2: Sketchs of the openings with all dimensions in mm.

Flow Id	h_1(m)	Q_u(L/s)	Fr_1	Re_1
F_1	0.025	2.0	0.2	9,524
F_2	0.108	17.6	0.2	69,980
F_3	0.025	5.4	0.55	25,714
F_4	0.090	36.7	0.55	151,340
F_5	0.108	46	0.52	182,903

Table 1: Tested flow configurations (at laboratory scale)

4.3 Tested flow configurations (F)

Four different flow configurations are selected to reproduce four flood events: two with a high and two with a low street slope (typically 1/1000 and 1/100); two with a high and two with a low water level (typically 30cm and 1.2m), as given in Table 1, with the Froude number $Fr_1 = Q_u/(bh_1\sqrt{gh_1})$ and Reynolds number $Re_1 = 4Q_u/[(b+2h_1)\nu]$

F_1 and F_2 are flow configurations with a low Froude number (corresponding to a low slope urban area) while F_3, F_4 and F_5 are configurations with a high Froude number (corresponding to a high slope urban area). F_1 and F_3 are configurations with a low water depth (2.5 cm at laboratory scale that is 12x2.5 = 30 cm at real scale) while F_2, F_4 and F_5 are configurations with a high water depth (about 10 cm at laboratory scale that is 12x10 = 1.2 m at real scale).

4.4 List of obstacles

As for openings, the analysis of street photographs permitted to list the most common obstacles encountered in the streets and on the facades. For sake of simplicity, we brought together all obstacles having the same typical size and location with regards to the street and the opening. Note that only big enough and fixed obstacles are considered herein. Mobile obstacles such as waste containers, potted plants can also affect the flow intrusion if they are

Id	Elements	Description
0	n/a	No obstacle
	1 : Car(s) or bus shelter(s)	
1a-up	13	Unique car at the upstream end of the opening
1a-cent	10	Unique car facing the opening
1a-dw	14	Unique car at the downstream end of the opening
1a-mid	15	Unique car in the middle of the street
1b-1	8+9+10+11+12	Row of parked cars with one car facing the opening
1b-2	1+2+3+4+5	1b-1 staggered with regards to the opening
1b-2-up	1+2+3+4+5+6	1b-2 with one car added in the middle of the street upstream
1b-2-dw	1+2+3+4+5+7	1b-2 with one car added in the middle of the street downstream
	2 : Facade detail(s) (e.g. tree, utility pole, mailbox...) on the sidewalk near the facade	
2a-up	18	Facade detail upstream from the opening
2a-dw	19	Facade detail downstream from the opening
2b	16+17+18+19+20	A row of facade details
2c	18+19	A couple of facade details
	3 : Street detail(s) (e.g. tree, utility pole, street light, traffic sign...) on the sidewalk near the traffic lane	
3a-up	23	A street detail upstream from the opening
3a-cent	24	A street detail facing the opening
3a-dw	25	A street detail downstream from the opening
3b	21+22+23+24+25+26	A row of street details
	4 : Additional obstacles	
4a	27	A porch
4b	28	A windowsill
4c	29	A stair

Table 2: List of the 19 tested obstacle configurations; see Fig. 3 for the shape, size and location of each individual obstacle element.

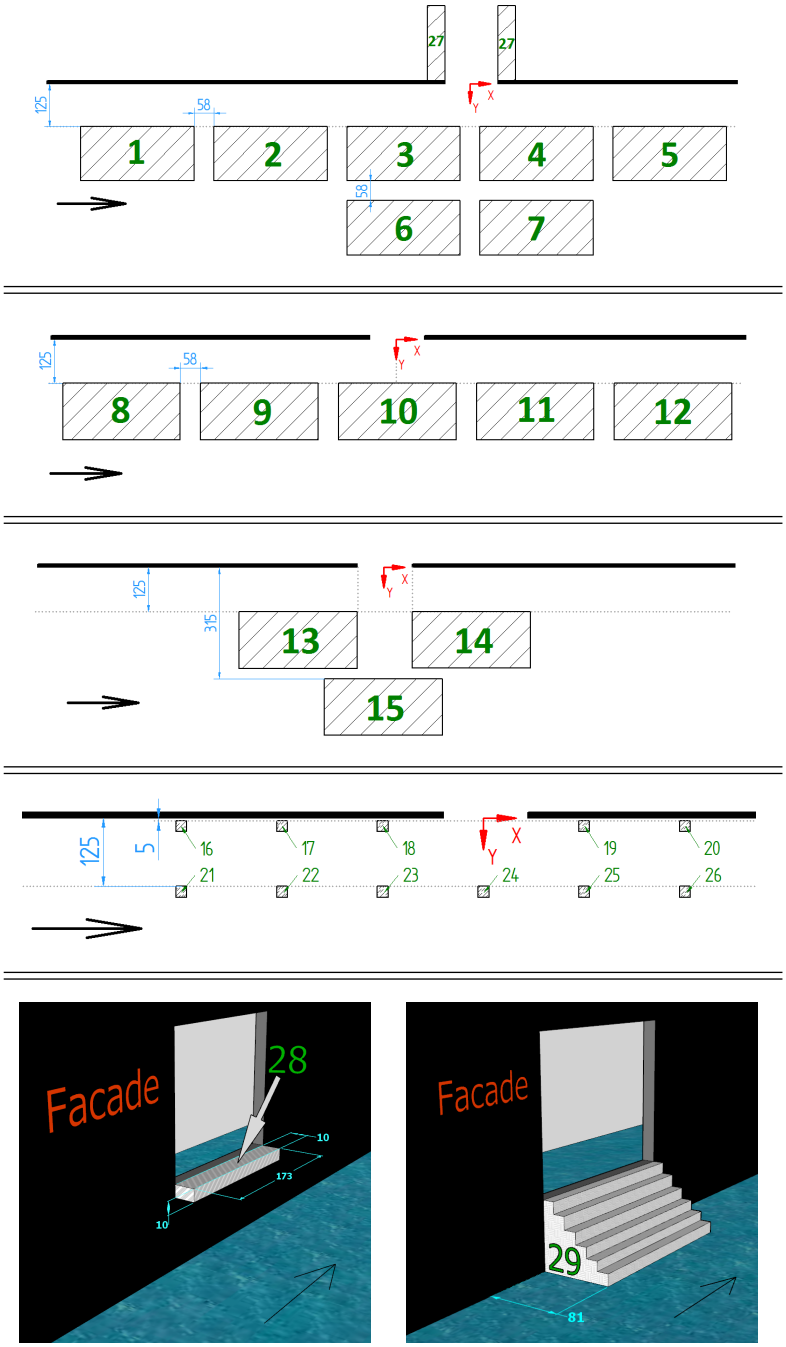

Figure 3: Sketches of all obstacles elements. Their sizes are: for elements 1 to 15 : $Lx = 335$ mm, $Ly = 162$ mm; for elements 16 to 26 : $Lx = Ly = 20$ mm; for elements 27 : $Lx = 52$ mm, $Ly = 220$ mm, with Lx and Ly the dimensions along x and y axes respectively.

transported by the flow and partially block the opening, but mobile obstacles are not considered herein. Moreover, for the highest water levels and flow velocity magnitudes, some obstacles such as parked cars are expected to be set in motion (Smith et al., 2019), either blocking the opening or being swept away further downstream. However, this effect is not considered herein for sake of simplicity. We end-up with four main types of obstacles:

1. **Cars/bus shelters**, noted "1" as Id in Table 2 : These are parked cars or bus shelters classically located on or just adjacent to the sidewalk, in front of building facades.

2. **Facade details**, noted "2" as Id in Table 2 : These are trees, utility poles, mailboxes and all other obstacles located on the sidewalk close to the facade. These obstacles are usually of relatively small horizontal size.

3. **Street details**, noted "3" as Id in Table 2 : These are trees, utility poles, street lights, traffic signs and all other obstacles located on the sidewalk near the traffic lane. These obstacles are assumed to be of same typical size as facade details.

4. **Additional obstacles**, noted "4" as Id in Table 2 : These are all obstacles that do not fit in the three previous types; here we consider a porch inside the building area, a windowsill attached to the facade and stairs to access elevated doors.

Following this typology, 19 obstacle configurations (plus 7 combinations, see below) are selected and listed in Table 2. These obstacle configurations are composed of 1 to 6 obstacle elements (listed as 2^{nd} column of Table 2) which shapes, dimensions and locations are sketched on Fig. 3). Some obstacle configurations comprise a single obstacle (a car, a tree, a mailbox, a porch...), others comprise couples or alignments of individual obstacles (a couple/row

of park cars, of trees...) and finally more complex configurations include an additional fixed car in the middle of the street.

As sketched on Fig. 3, all obstacle elements have simplified shapes. Apart from two obstacles of type 4 (the windowsill and stair), they are all rectangular prisms, mounted on the bottom of the flume and emerging across the free-surface. Large obstacles elements (1 to 15 + 27) are made of impervious bricks (see also Fig.4a) and smaller obstacles (16 to 26) of impervious square bars. The dimensions of the obstacles (indicated on Fig. 3) are selected to fit at most with real dimensions (according to the considered 1/12 scale): cars / bus shelters are 335 mm long and 162 mm wide (about 4 x 2 m at real scale); street and facade details are 20 mm square base (24 cm at real scale). Fig.4 depicts three examples of obstacle configurations.

4.5 Measurement uncertainties and scale effects

For a given flow configuration, the uncertainties regarding the measured intrusion discharge Q_w are related to:

- uncertainties regarding the exact location of obstacle. To evaluate this source of uncertainties, three obstacles configurations are added and removed three times for two flow conditions ($F1$ and $F4$) with opening $Op2$. Typical variations of the intrusion discharge among the three repetitions equal 0.91% for the flow with low Froude number and 0.93% with the high Froude number.

- the measurement method used to estimate the intrusion discharge. Q_w is measured using a triangular weir for which the water depth upstream from the weir is measured by an ultrasonic probe and the discharge is computed using the previously calibrated rating curve. Uncertainties regarding the measured water depth is estimated by repeating (at different

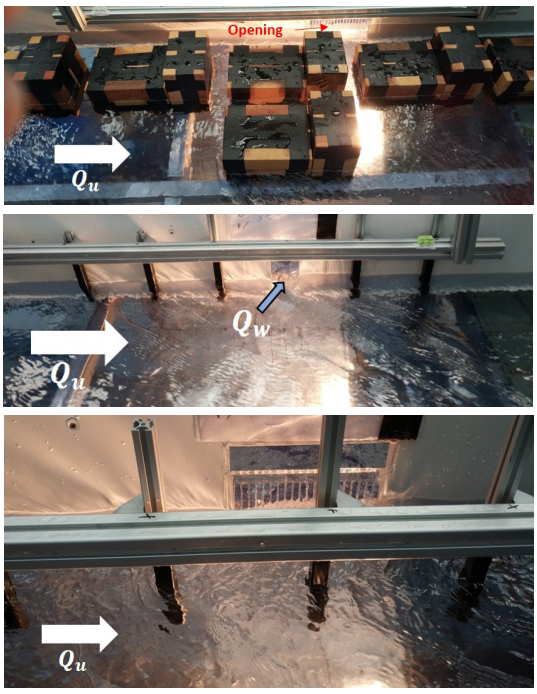

Figure 4: Photographs of three obstacle configurations: (a) = parked cars (obstacle 1b-2-up), (b) = facade details (obstacle 2b) and (c) = street details (obstacle 3b). Note that the horizontal bar on (b) and (c) permits to maintain the obstacle steady and remains above the free-surface.

times) several same flow/opening/obstacle configurations. The variability between the measured water depths remains smaller than 1.8% for the low Froude number cases and 2.0% for the high Froude number cases. Moreover, uncertainties reported when establishing the calibration curve of the triangular weir is about 1.5% for the measured discharge.

In the end, the measured intrusion discharge uncertainty does not exceed 3%. Note that by sake of clarity, results graphs in the sequel do not contain errorbars related to this level of uncertainty.

Moreover, scale effects are expected to distort the extrapolation of the measurements obtained on the present small-scale model (1:12) to the real (prototype) scale. Indeed, while the length ratios and Froude number are at scale with real events, the Reynolds numbers considered herein (Table 1) are much lower than those of real scale. Using a Froude similarity, the prototype Reynolds number is expected to be $12^{3/2}$ times higher than the model Reynolds number. Similarly, the Weber number We, accounting for the influence of surface tension, will vary. Above the windows crest, We is estimated smaller than about 100 in the experiments, indicating that some capillary effects can affect present results. They will be absent at the prototype scale. Indeed, assuming roughly that the inlet discharge is correctly estimated by a De Marchi formula (Eq.1) with a constant discharge coefficient, the prototype Weber number will be 12^2 times higher than in experiments. Care should thus be taken when extrapolating the present results to real scale flood events.

4.6 Methodology

Note that all openings are studied for the flows without obstacle, while only three openings ($Op1$, $Op2$ and $Op4$) are used with obstacles. Moreover, for the elevated openings ($Op1$, $Op3$ and $Op4$) the low water level for flows $F1$

and $F3$ does not reach the opening and these configurations are discarded. To summarize, we measure the flow intrusion for 10 combinations of flow/openings without obstacles and 8 combinations of flow/openings with the 26 obstacle configurations (except for obstacles $4b$ only used with the window ($Op1$) and $4c$ only used with the door ($Op2$)).

For each combination of flow and opening configuration, the following strategy is employed:

1. The boundary conditions are adjusted according to Table 1: the upstream discharge Q_u and the weir crest height to reach the desired water depth. This flow is labeled "0", i.e. without obstacle, in the sequel. The intrusion discharge is recorded.

2. Each obstacle configuration is installed in the channel one after the other and the intrusion discharge is recorded once the steady state is reached. It is verified that h_1 hardly varies when changing the obstacles.

5 Flow configurations without obstacles

Present results section depicts the intrusion flow from the flooded street to the building area in absence of any obstacle in the street or on the facade.

5.1 Flow description

Fig. 5(a) depicts the surface velocity field in the street near the opening, for flow $F2$ with opening $Op2$ and Fig. 6(a) depicts the 2D field of water elevation field for flow $F4$ with opening $Op2$. In such condition, the flow pattern is very similar to canonical flow configuration at a rectangular side weir. As expected, when approaching the opening section, the surface velocity increases and rotates towards the opening, while the velocity downstream the opening strongly

decreases. Due to the intrusion discharge leaving the street side, the discharge in the street decreases towards downstream so that the mean velocity in the sections downstream the opening is smaller than that upstream. Moreover, the water depth field shows a local depression with low water levels near the upstream corner of the opening and a local maximum of water level near the downstream corner. This behavior is in agreement with previously measured water level profiles along rectangular side weirs, as that from Bagheri et al. (2013).

5.2 Discharge equation

The prediction of intrusion discharge through a rectangular side weir adjacent to a straight and smooth rectangular channel, has been performed by many authors (listed in Table 3) since the 1970's. Emiroglu et al. (2011) listed more than 1500 measured intrusion discharges available in the literature. Most authors proposed semi-empirical formulas permitting to predict the intrusion discharge using the classical De Marchi (1934) equation:

$$C_{\mathrm{d}} = \frac{(3/2)Q_{\mathrm{w}}}{\sqrt{2\mathrm{g}}(h_1 - \mathrm{p})^{3/2}\mathrm{L}} \tag{1}$$

where p is the crest height, L the length of the lateral weir, and h_1 the water depth at the upstream section of the opening along the center of the channel. The authors then proposed semi-empirical formulas for the discharge coefficient (C_d) based on the non-dimensional parameters that arise from the dimensional analysis: Fr_1, p/h_1 and L/b, with b the channel width. Table 3 lists 12 among the best known available formulas for coefficient C_d (made more and more complex along time) along with the ranges of parameters used for fitting their formulas. For sake of comparison, the three last lines of Table 3

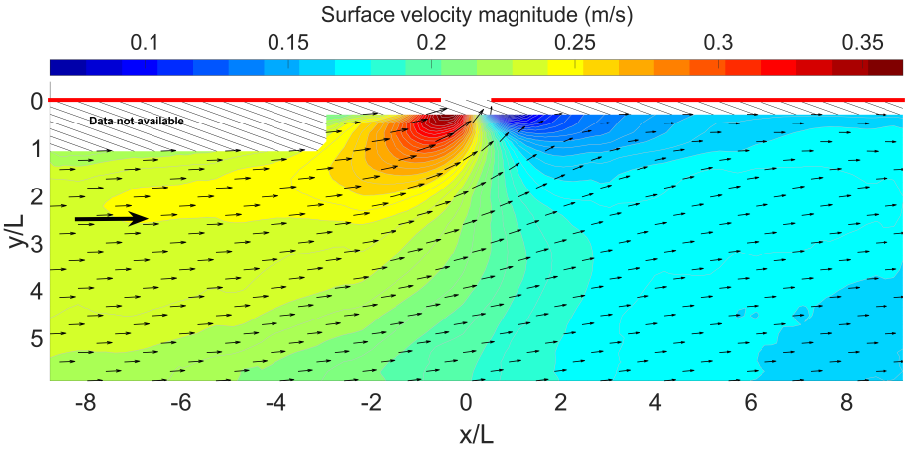

(a) Without obstacle

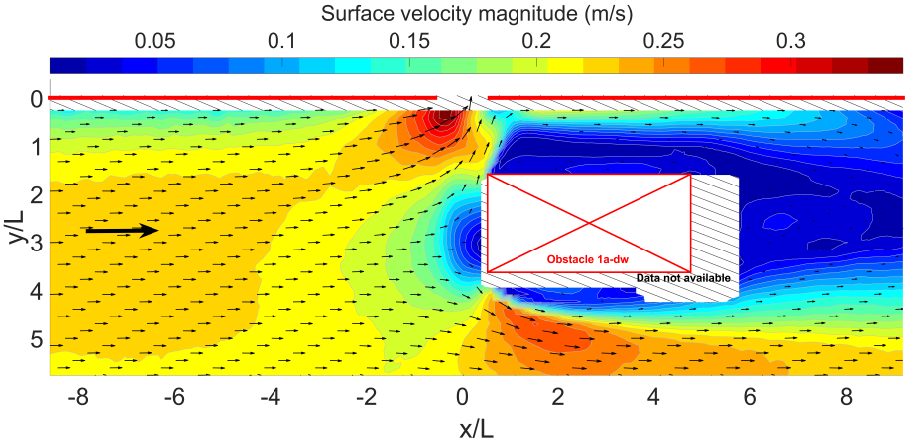

(b) With obstacle 1a-dw

Figure 5: Surface velocity fields for flow configuration $F2$ and opening $Op2$ (the door) without (a) and with (b) obstacle 1a-dw.

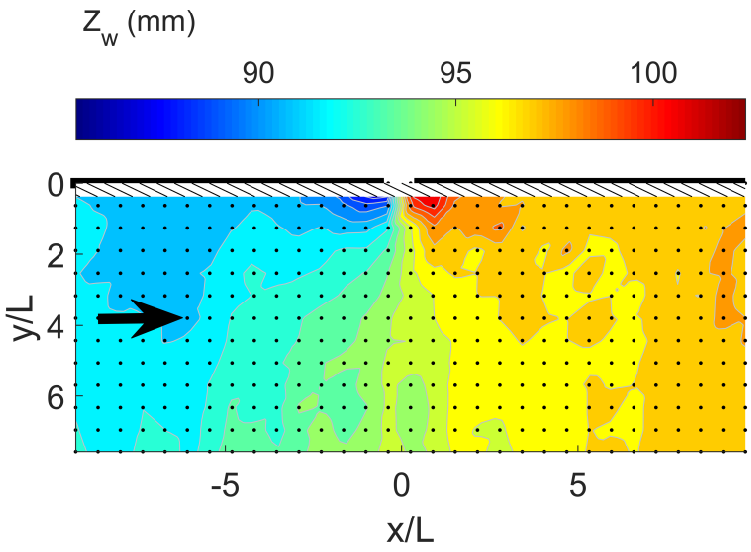

(a) Without obstacle

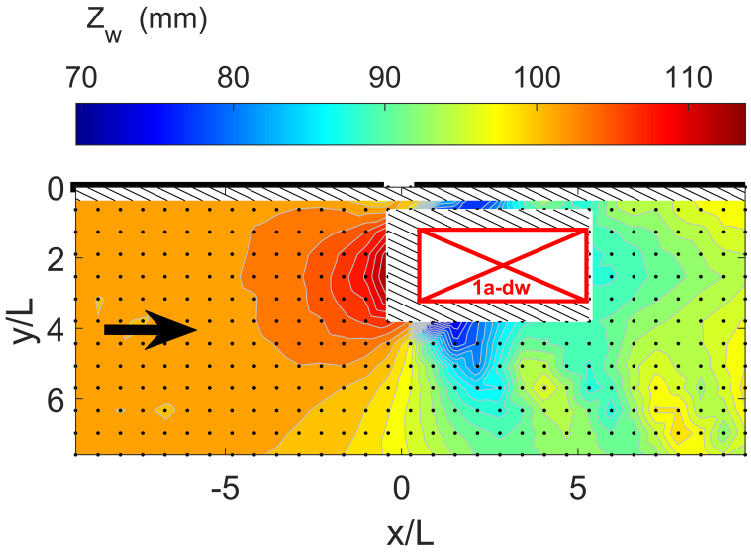

(b) With obstacle 1a-dw

Figure 6: Elevation of the free-surface with regards to the channel bed at the center of the opening ($x/L = 0$; $y/L = 0$) for flow configuration $F4$ and opening $Op2$ without (a) and with (b) obstacle 1a-dw. Black dots correspond to the measurement grid points.

comprise the range of parameters of our experimental campaigns (see Table. 1).

Source	Discharge coefficient C_d	Fr_1	p/h_1	L/b
Nandesamoorthy and Thomson (1972)	$C_d = 0.432\left(\frac{2+Fr_1^2}{1+2Fr_1^2}\right)^{0.5}$	0.02-4.3	0-0.96	0.2-1.0
Subramanya and Awasthy (1972)	$C_d = 0.611\left(1-\frac{3Fr_1^2}{2+Fr_1^2}\right)^{0.5}$	0.02-4.3	0-0.96	0.2-1.0
Yu-Tech (1972)	$C_d = 0.622 - 0.222Fr_1$	0.02-4.3	0-0.96	0.2-1.0
Ranga Raju et al. (1979)	$C_d = 0.81 - 0.6Fr_1$	n/a	n/a	0.2-1.25
Hager (1987)	$C_d = 0.485\left(\frac{2+Fr_1^2}{2+3Fr_1^2}\right)^{0.5}$	0.3-2	n/a	3.33
Singh et al. (1994)	$C_d = 0.33 - 0.18Fr_1 + 0.49\frac{p}{h_1}$	0.22-0.45	0.45-0.85	0.4-0.8
Swamee et al. (1994a)	$C_d = 0.447\left[\left(\frac{44.7p}{49p+h_1}\right)^{6.67} + \left(\frac{h_1-p}{h_1}\right)^{6.67}\right]^{-0.15}$	0.10-0.93	0-1.25	0.4-1
Swamee et al. (1994b)	$C_d = 1.06\left[\left(\frac{14.14p}{8.15p+h_1}\right)^{10} + \left(\frac{h_1}{h_1+p}\right)^{15}\right]^{-0.1}$	0-0.6	0-1	n/a
Jalili and Borghei (1996)	$C_d = 0.71 - 0.41Fr_1 - 0.22\frac{p}{h_1}$	0.1-2	0.05-0.87	0.67-2.5
Borghei et al. (1999)	$C_d = 0.7 - 0.48Fr_1 - 0.3\frac{p}{h_1} + 0.06\frac{L}{b}$	0.1-0.9	0.02-0.87	0.67-2.33
Emiroglu et al. (2011)	$C_d = \left[0.836 + \left(-0.035 + 0.39\left(\frac{p}{h_1}\right)^{12.69} + 0.158\left(\frac{L}{b}\right)^{0.59} + 0.049\left(\frac{L}{h_1}\right)^{0.42} + 0.244Fr_1^{2.125}\right)^{3.018}\right]^{5.36}$	0.08-0.92	0.34-0.91	0.30-3.00
Bagheri et al. (2013)	$C_d = -1.423Fr_1^{0.138} + 0.744\left(\frac{h_1-p}{L}\right)^{-0.083} + 0.723\left(\frac{h_1-p}{p}\right)^{0.088} + 0.182\left(\frac{L}{b}\right)^{-0.241}$	0.08-0.91	0.22-0.9	0.5-1.5
Present study (Op1)	-	0.2-0.52	0.77	0.19
Present study (Op2)	-	0.2-0.55	0	0.1
Present study (Op3)	-	0.20-0.52	0.62	0.26

Table 3: Existing equations for the side weir discharge coefficient (C_d) and corresponding tested parameters (plus present range of parameters; note that Op 4 is not indicated here due to its specific geometry)

In order to test the validity of the formulas from Table 3, Fig. 7 plots ΔQ_w, the error in predicted intrusion discharge compared to present measurements. The general agreement is quite poor, as could be expected given the low agreement between these formulas already mentioned by Emiroglu et al. (2011). Nevertheless, Swamee et al. (1994b) formula appears to perform well (averaged error of 6%) for predicting the intrusion discharge through open windows (Op1 and Op3) while formulas from Nandesamoorthy and Thomson (1972), Yu-Tech (1972) and Jalili and Borghei (1996) appear to perform well (averaged error of 10%) for the intrusion discharge through the door (Op2).

6 Impact of obstacles on the flow intrusion

As discussed above, flow intrusion from a flooded street to an adjacent building area is made more complicated than a classical rectangular side weir due to the presence of obstacles in the street and on the facade. The aim of present section is then to identify the effect of such obstacles on the flow pattern near the opening and on the intrusion flow discharge.

6.1 Flow description

Fig. 5(b) depicts the impact of a single car parked just downstream an open door on the surface velocity field near the door ($Op2$) for flow $F2$. As expected low velocity regions are measured upstream, downstream and on the side of the obstacle. Indeed, flow detachment on the side and downstream from the car is enhanced by the sharp corners of the obstacle. The flow approaching the obstacle rotates towards both sides: towards the open door on the left side and towards the center of the street on the right side of the obstacle. This behavior is very similar to that measured by Mignot et al. (2013) around standing obstacles in the middle of flooded crossroads. Moreover, Fig. 6(a) and (b) compares the

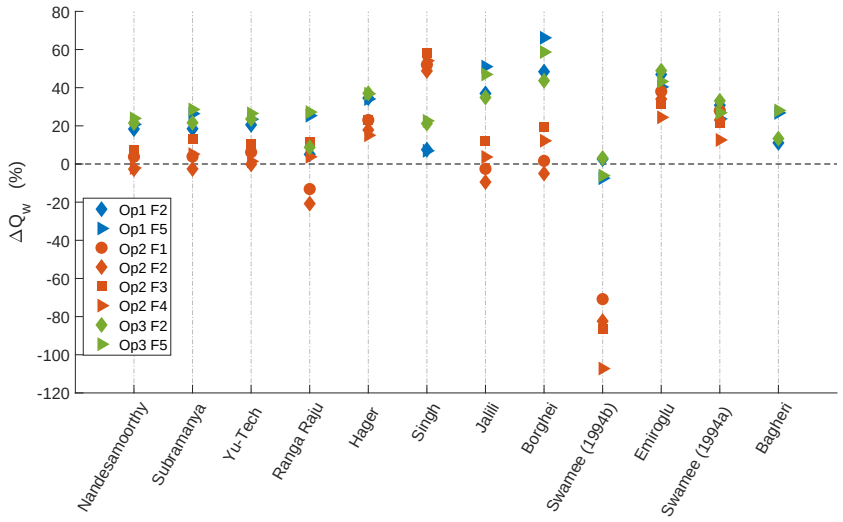

Figure 7: Relative difference between Q_w calculated with the semi-empirical law from Table 3 and measured Q_w (without obstacle).

free surface elevation with and without this parked car for a flow with a higher Froude number. As expected, the water level is increased in front of the car and decreased on its sides. Globally, the whole flow pattern in the vicinity of the obstacle appears to be strongly affected by the obstacle, so that the corresponding intrusion flow discharge is also expected to be much affected.

6.2 Impact of obstacles on the intrusion discharge

The aim of present section is to quantify the impact of obstacles on the intrusion discharge toward the building area. The relative difference between intrusion discharge with an obstacle O_i and without any obstacle, for the same opening and flow configuration reads: $\Delta Q_w = \frac{Q_{w,i} - Q_{w,0}}{Q_{w,0}}$, where subscript 0 refers to the configuration without obstacle. Fig. 8 plots the impact of the 26 obstacle configurations on the 8 tested flow configurations (openings / flow conditions) and reveals that the obstacles impact the intrusion discharge up to +/- 100 %.

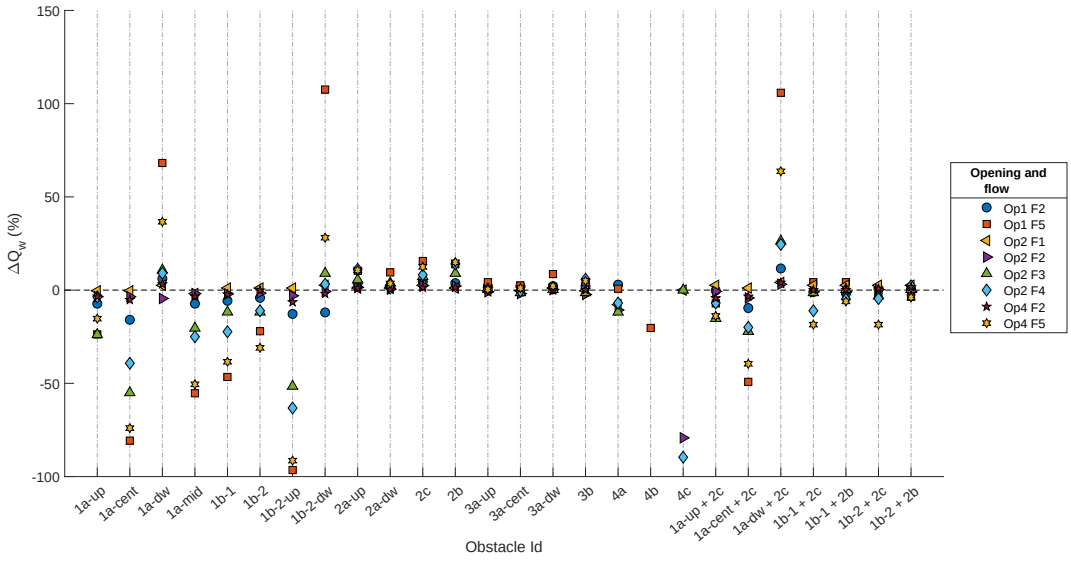

Figure 8: Overview of the impact of the obstacles on the intrusion discharge.

Moreover, some obstacles increase ($\Delta Q_w > 0$) while others decrease ($\Delta Q_w < 0$) the intrusion discharge. As expected, the large obstacles (cars / bus shelters, assumed to remain fixed for sake of simplicity) have a more significant impact than the smaller obstacles (facade and street details). On the other hand, for a given obstacle configuration (a given abscissa on the figure), the sign of ΔQ_w mostly stays the same for the 8 flow configurations, except for some given obstacles (e.g. $1a - dw$ or $1b - 2 - dw$).

A deeper analysis on these impacts is proposed in the next section with the influence of (i) the position of the obstacle with regards to the opening, (ii) the Froude number and (iii) the non-dimensional water depth of the approaching flow in the street and (iv) finally the type of opening.

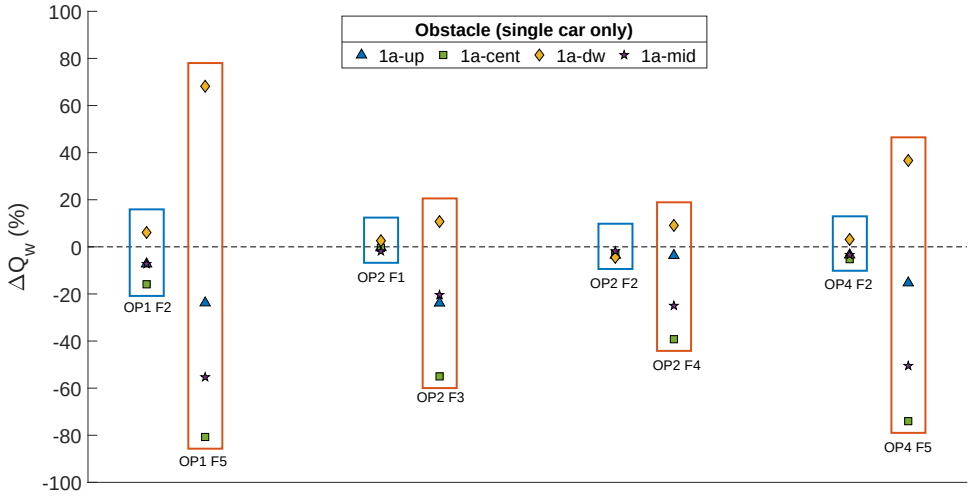

Figure 9: Impact of the position of a single car (1a-up, 1a-cent, 1a-dw and 1a-mid) on Q_w. Orange rectangles highlight the flow configurations with a high Froude number while blue rectangles highlight the flows with a low Froude number.

6.2.1 Influence of the position of the obstacle (single cars)

Fig. 9 plots ΔQ_w for the four single car configurations (with the car located upstream (*up*), in front of (*cent*), downstream (*dw*) from the opening or in the middle of the street (*mid*). The figure shows that the location of the obstacle strongly affects the intrusion discharge with a positive ΔQ_w when the car is located downstream from the opening and a negative value for the other locations. As expected, the intrusion is particularly reduced when the car is located just in front of (i.e. blocking) the opening. Moreover, the variability of the influence of a single parked car location is very high (up to +/- 80%), i.e. of same order as the intrusion discharge itself.

6.2.2 Influence of the Froude number

In Fig. 9, ΔQ_w is split as a function of the Froude number: blue boxes refer to flow configurations with a low Froude number while red boxes refer to flow configurations with a high Froude number. The tendendy is similar for the 4 opening / water depth configurations: the modification of intrusion discharge is much larger with the higher Froude number.

To get a more quantified effet of the Froude number, Fig. 10 plots, for the four same opening/water depth configurations, the absolute value of ratio $\Delta \mathrm{Q_w}$ between the high and low Froude numbers for the 26 obstacle configurations with :

$$\Delta \mathrm{Q_w \ ratio} = \frac{\Delta \mathrm{Q_{w,\ High\ Froude\ number}}}{\Delta \mathrm{Q_{w,\ Low\ Froude\ number}}} \tag{2}$$

In agreement with Fig. 9, the modification of intrusion discharges usually increases as the Froude number increases, and this increase can reach up to 100%. However, for some configurations the increasing Froude number decreases the impact of the obstacle. But, more interestingly, for these obstacles configurations, the increasing Froude number either increase or decrease the obstacle impact on $\Delta \mathrm{Q_w}$ depending of the flow and the opening properties. For instance, in the case of the street detail centered in front the door ($3a - cent$ with $Op2$)ΔQ_w ratio is below 1 for flow cases with a high water depth ($F2$ & $F4$) but above 1 with a low water depth ($F1$ & $F3$).

6.2.3 Influence of the water depth

This section aims at establishing how the impact of obstacles is affected by the water depth. This analysis can only be performed for the door ($Op2$), as for the elevated openings, the low water depth does not lead to any flow intrusion.

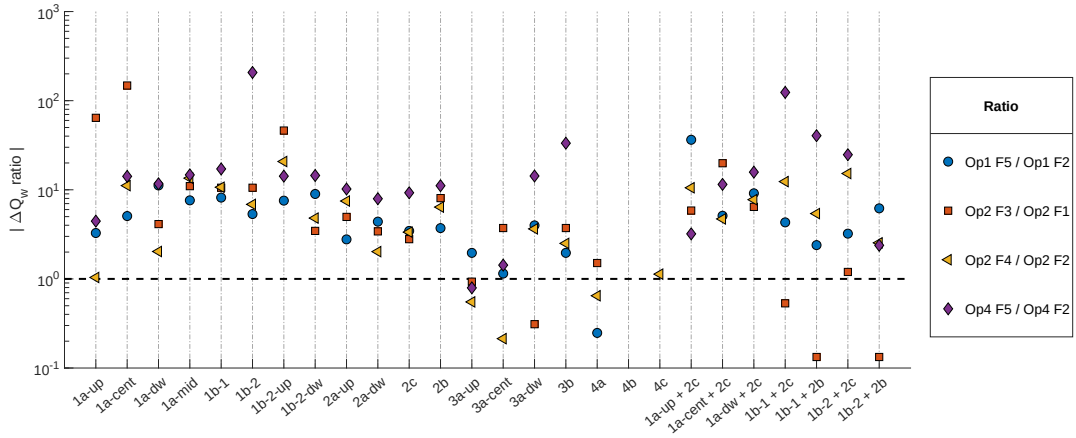

Figure 10: Impact of the Froude number on the modification of intrusion discharge due to an obstacle configuration.

Fig. 11 compares the intrusion discharges with low and high water depths for two configurations (with low and high Froude number) using $\Delta Q_w ratio$:

$$\Delta \mathrm{Q_w\ ratio} = \frac{\Delta \mathrm{Q_{w,\ High\ water\ depth}}}{\Delta \mathrm{Q_{w,\ Low\ water\ depth}}} \tag{3}$$

The impact of obstacles appears to be strongly affected by the water depth, some ratios reaching up to 10 (or 1/10). However, no main tendency arises from this analysis.

6.2.4 Influence of the type of opening

Finally, the absolute value of obstacle impact on the intrusion discharge $|\Delta \mathrm{Q_w}|$ is plotted on Fig. 12 for the three openings (for the flow configuration with a high Froude number and a high water depth). For most obstacle configurations, the impact of the obstacle on the intrusion discharge is maximum for the window (Op 1), then for the door (Op 2) and finally the gate (Op 4). This result

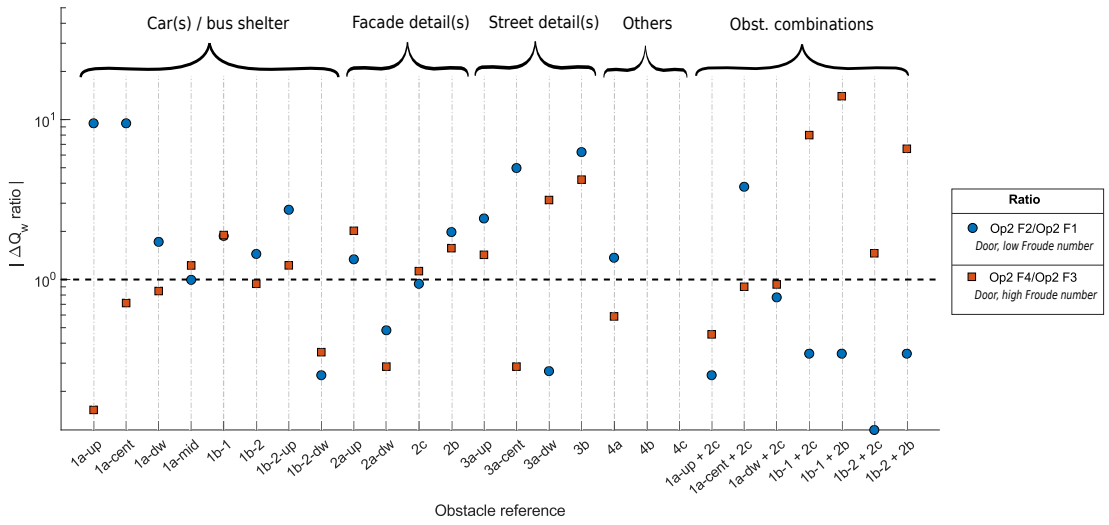

Figure 11: Impact of the water depth on the modification of the intrusion discharge due to the obstacles.

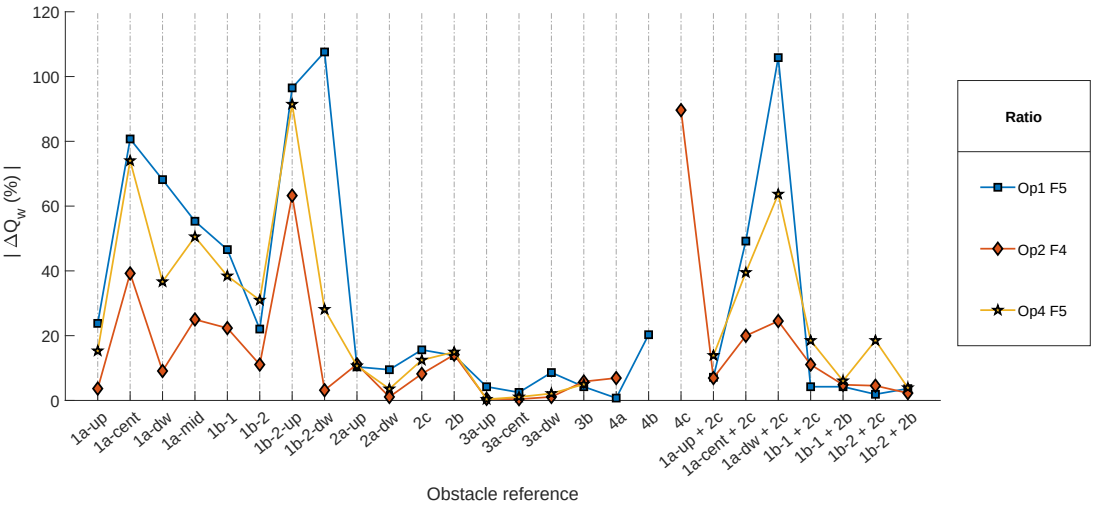

Figure 12: Impact of the type of opening on the intrusion discharge.

is logical as a given water depth fluctuation induced by the presence of an obstacle promotes a higher relative variation above an elevated side weir (i.e. the window) than above a mounted opening (i.e. the door). This is consistent with differences that are higher when the obstacle is located downstream (i.e. for configurations 1a-dw, 1b-2-dw and 1a-dw+2c).

6.3 Impact of the obstacle shape simplification

As exposed above, all obstacles have a highly simplified shape, they are rectangular prism, mounted on the bed and emerging across the free-surface. To estimate the effect of simplifying the shape of the obstacles, a realistic car of scale 1:12 is inserted (fixed on the bed), either looking upstream ("Car-up") or downstream ("Car-dw"), at the same location as obstacle configuration 1a-mid (that is obstacle element 15 in Fig. 3). The impact of the realistic car on the intrusion discharge is compared to that of the simplified shape obstacle with the door as opening ($Op2$) for two flows with high water depths.

While all three obstacles hardly impact the intrusion discharge for the low Froude number, with the high Froude number the intrusion discharge highly differs between the realistic and simplified shapes and in a lesser extent with the car orientation. These differences are attributed to the water passing below the car, which is not the case for the simplified obstacle shapes that mimic with higher fidelity the bus shelters. These results do not affect the conclusions of present sensitivity analysis that exhibits a variability of several tens of percent of the intrusion discharge in presence/absence of obstacles. However, they show that a quantitative estimate of the intrusion discharge for a particular opening/obstacle case would require realistic ad-hoc models of furniture/face details.

(a) Realistic car

(b) Car-dw

(c) Car-up

Figure 13: Photographs of the realistic parked car, looking upstream and downstream

Obstacle	Q_w (L/s)		ΔQ_w (%)	
	$\mathbf{F_2}$	$\mathbf{F_5}$	$\mathbf{F_2}$	$\mathbf{F_5}$
0	4.19	3.49	-	-
1a-mid	4.11	3.29	-1.91	-5.73
Car-dw	4.03	2.91	-3.82	-16.62
Car-up	4.09	2.96	-2.39	-15.19

Table 4: Comparison of the intrusion discharge (Q_w) and the effect of obstacle (ΔQ_w) using realistic parked cars looking downstream (Car-dw) and upstream (Car-up) and the simplified shape obstacle 1a-mid.

7 Discussion and conclusions

This work aimed at investigating the flow processes involved as a flow passes from a flooded street to an adjacent building area via an opening in the facade and measuring the corresponding discharge. Three openings and four flow regimes were tested. Moreover, 26 obstacle configuration, representative of typical obstacles encountered in streets were included for three of the openings to assess the impact of these obstacles on the intrusion discharge.

It was observed that the flow pattern through an opening is quite similar to that over a lateral rectangular side weir, commonly described in the litera-

ture. The semi-analytical laws available in the literature to predict the intrusion discharges were then tested for the flow configurations without obstacles. It appears that, while some equations fairly agree with present measurements for the flows through doors (Nandesamoorthy and Thomson (1972), Yu-Tech (1972) and Jalili and Borghei (1996) with a typical difference of 10%) and others through windows (Swamee et al. (1994b) with a typical difference of 6%), other equations strongly over- or under-estimate the intrusion discharge (by up to 100%).

When adding obstacles, the flow pattern and intrusion discharge are affected. The impact of the obstacles strongly depends on the following parameters: the location of the obstacle(s) with regards to the opening, the Froude number and water depth of the approaching flow in the street and the characteristics of the opening. Globally:

- Urban furniture (without parked cars) affect the intrusion discharge (increasing or decreasing it) by about 12% (for doors) to 15% (for windows) when the Froude number is high (≈ 0.5) and about 3% (for doors) to 5% (for windows) when the Froude number is lower (≈ 0.2).

- Obstacles miming parked cars or bus shelters (with or without urban furniture) affect the intrusion discharge by about 50% (for doors) to 80% (for windows) when the Froude number is high and about 5% (for doors) to 15% (for windows) when the Froude number is lower.

This work then permitted to evaluate the level of variability of the intrusion discharge towards a building with regards to the hydraulic and geometric parameters of the flooded street and of the opening and to the type of obstacle that can be encountered during urban floods. It provides an estimate of the errors made by numerical computations according to the degree of details of the street/facade geometry.

Finally this database, gathering 220 measured intrusion discharges, is now available for the inclusion and calibration of analytical/empirical equations in operational models adapted to simulate urban floods. Including openings in these models would however require to identify their locations along with their characteristics (width, crest elevation...) along the facades. This information is sometimes available in GIS data bases of the cities, or would have to be located using photographs such as in "Google Street View". Regarding the impact of obstacles on the flow discharge, a simple, first step would be to identify the facades in front of which cars parking is permitted, and to consider the effect of parked cars only for these openings.

Nevertheless, the approach presented herein was much simplified and thus present several major limitations. First, a single opening was considered while several neighboring openings on a facade may be damaged simultaneously. In this case, the intrusion flow pattern towards one opening is expected to be affected by the intrusions through the openings located upstream. Second, openings considered herein are expected to be removed by the flow, leaving a large rectangular open space for the flow intrusion. In the reality, the openings are expected to be only partially damaged and more complex shapes of open spaces are expected to be encountered. Third, in the present work, no backward effect of the flow within the building area is considered: the intrusion flow through the opening remains similar to that over an unsubmerged side weir. In a real situation, the storage capacity of a building and the outflows from the building to a neighboring street through another opening are limited, so that stored volume of water is expected to affect the intrusion discharge (in the same way as for a partially submerged side weir). Fourth, some obstacles not-attached to the ground such as trash containers, potted plants, cars (Smith et al., 2019)... can be mobile under high flow levels and, if partially blocking the openings could

also affect the intrusion discharges. Fifth, in some wide streets, the width of the sidewalk can be large enough so that the effect of the parked cars on the flow intrusion dramatically reduces. Next step for the understanding of flow exchanges between streets and building areas during urban floods will then be to consider experimental set-ups that represent small urban districts where the building areas are connected to several surrounding streets with various openings, as proposed by Mejia Morales et al. (in press).

8 Acknowledgments

This work has been supported by the French National Research Agency (ANR) under the grant ANR-18-CE01-0020. Authors are also grateful to C. Marmounier for the design and building of the experimental set-up.

References

Baba, Y., Ishigaki, T., Toda, K., 2017. Experimental studies on safety evacuation from underground spaces under inundated situations. Journal of JSCE 5, 269–278.

Bagheri, S., Kabiri-Samani, A., Heidarpour, M., 2013. Discharge coefficient of rectangular sharp-crested side weirs Part I: Traditional weir equation. Flow Measurement and Instrumentation 35, 109–115. doi:10.1016/j.flowmeasinst.2013.11.005.

Bazin, P.H., Mignot, E., Paquier, A., 2017. Computing flooding of crossroads with obstacles using a 2d numerical model. Journal of Hydraulic Research 55, 72–84.

Borghei, S., Jalili, M., Ghodsian, M., 1999. Discharge coefficient for sharp-crested side weir in subcritical flow. Journal of Hydraulic Engineering 125, 1051–1056.

Chang, T.J., Wang, C.H., Chen, A.S., Djordjević, S., 2018. The effect of inclusion of inlets in dual drainage modelling. Journal of Hydrology 559, 541–555.

Chen, Y., Zhou, H., Zhang, H., Du, G., Zhou, J., 2015. Urban flood risk warning under rapid urbanization. Environmental Research 139, 3–10. doi:10.1016/j.envres.2015.02.028.

De Marchi, G., 1934. Essay on the performance of lateral weirs. L'Energia Elettrica, Milan, Italy 11, 849–860.

Emiroglu, M.E., Agaccioglu, H., Kaya, N., 2011. Discharging capacity of rectangular side weirs in straight open channels. Flow Measurement and Instrumentation 22, 319–330. doi:10.1016/j.flowmeasinst.2011.04.003.

Fang, Q., 2016. Adapting Chinese cities to climate change. Science 354, 425–426. doi:10.1126/science.aak9826.

Gems, B., Mazzorana, B., Hofer, T., Sturm, M., Gabl, R., Aufleger, M., 2016. 3-d hydrodynamic modelling of flood impacts on a building and indoor flooding processes. Natural Hazards and Earth System Sciences 16, 1351–1368.

Gross, M., 2016. The Urbanisation of Our Species. Elsevier.

Guha-Sapir, D., 2018. 2018 Review of Disasters Events. Technical Report. Centre for Research on the Epidemiology of Disasters, CRED.

Hager, W.H., 1987. Lateral outflow over side weirs. Journal of Hydraulic Engineering 113, 491–504.

Ishigaki, T., 2008. Evacuation criteria during urban flooding in underground space. Proc. of 11th ICUD, Scotland, UK, 2008 .

Jalili, M., Borghei, S., 1996. Discussion: Discharge coefficient of rectangular side weirs. Journal of Irrigation and Drainage Engineering 122, 132–132.

Liu, L., Sun, J., Lin, B., Lu, L., 2018. Building performance in dam-break flow - an experimental study. Urban Water Journal 15, 251–258.

Mejia Morales, M.A., Proust, S., Mignot, E., PaquierA., in press. Experimental and numerical modelling of the influence of street-block flow exchanges during urban floods. Advances in Hydroinformatics, Springer .

Mignot, E., Li, X., Dewals, B., 2019. Experimental modelling of urban flooding: A review. Journal of Hydrology 568, 334–342. doi:10.1016/j.jhydrol.2018.11.001.

Mignot, E., Paquier, A., Haider, S., 2006. Modeling floods in a dense urban area using 2d shallow water equations. Journal of Hydrology 327, 186–199.

Mignot, E., Zeng, C., Dominguez, G., Li, C.W., Rivière, N., Bazin, P.H., 2013. Impact of topographic obstacles on the discharge distribution in open-channel bifurcations. Journal of hydrology 494, 10–19.

Nandesamoorthy, T., Thomson, A., 1972. Discussion of spatially varied flow over side weir. ASCE Journal of the Hydraulics Division 98, 2234–2235.

Ranga Raju, K.G., Gupta, S.K., Prasad, B., 1979. Side weir in rectangular channel. Journal of the Hydraulics Division 105, 547–554.

Singh, R., Manivannan, D., Satyanarayana, T., 1994. Discharge coefficient of rectangular side weirs. Journal of Irrigation and Drainage Engineering 120, 814–819.

Smith, G.P., Modra, B.D., Felder, S., 2019. Full-scale testing of stability curves for vehicles in flood waters. Journal of Flood Risk Management , e12527.

Sturm, M., Gems, B., Keller, F., Mazzorana, B., Fuchs, S., Papathoma-Köhle, M., Aufleger, M., 2018. Experimental measurements of flood-induced impact forces on exposed elements, in: E3S Web of Conferences, EDP Sciences. p. 05005.

Subramanya, K., Awasthy, S.C., 1972. Spatially varied flow over side-weirs. Journal of the Hydraulics Division 98, 1–10.

Swamee, P., K. Pathak, S., Mohan, M., K. Agrawal, S., S. Ali, M., 1994a. Subcritical flow over rectangular side weir. Journal of Irrigation and Drainage Engineering 120, 212–217. doi:10.1061/(ASCE)0733-9437(1994)120:1(212).

Swamee, P.K., Pathak, S.K., Ali, M.S., 1994b. Side-weir analysis using elementary discharge coefficient. Journal of Irrigation and Drainage Engineering 120, 742–755.

Takayama, T., Takara, K., Toda, K., Fujita, M., Mase, H., Tachikawa, Y., Yoneyama, N., Tsutsumi, D., Yasuda, T., Sayama, T., 2007. Research works for risk assessment technology related to flood in urban area. Annuals of disasters prevention research 50 C.

UNISDR and CRED, 2015. The Human Cost of Weather-Related Disasters (1995-2015).

United Nations Population Division, 2018. Urban population (% of total population) - Data. https://data.worldbank.org/indicator.

Wu, Y., Zhong, P.A., Zhang, Y., Xu, B., Ma, B., Yan, K., 2015. Integrated flood risk assessment and zonation method: a case study in huaihe river basin, china. Urban Water Journal 78, 635–651.

Yu-Tech, L., 1972. Discussion of spatially varied flow over side weir. Journal of Hydraulic Engineering 98, 2046–2048.

Zhou, Q., Yu, W., Chen, A.S., Jiang, C., Fu, G., 2016. Experimental assessment of building blockage effects in a simplified urban district. procedia engineering. Procedia Engineering 154, 844–852.